ASME Journal of Applied Mechanics
Online journal at:
https://asmedigitalcollection.asme.org/appliedmechanics

Interplay of Dry and Capillary Adhesion in Elastic Solids and Structures

Huang Lu
College of Mechanics and Engineering Science,
State Key Laboratory for Turbulence
and Complex Systems,
Peking University,
Beijing 100871, China
e-mail: 2100011022@stu.pku.edu.cn

Jin Qian
College of Mechanics and Engineering Science,
State Key Laboratory for Turbulence
and Complex Systems,
Peking University,
Beijing 100871, China
e-mail: jqian@zju.edu.cn

Zhaohe Dai[1]
College of Mechanics and Engineering Science,
State Key Laboratory for Turbulence
and Complex Systems,
Peking University,
Beijing 100871, China
e-mail: daizh@pku.edu.cn

Dry adhesion between solids relies on direct surface–surface interactions (such as van der Waals forces) that require intimate contact. In contrast, capillary adhesion occurs when a liquid bridge forms between surfaces and generates attractive forces through the line force and negative Laplace pressure. At first glance, these two adhesion mechanisms appear mutually exclusive or at least fundamentally different in origins, raising the question: When a liquid bridge brings two solid surfaces into contact, does the system exhibit dry or capillary adhesion as the bridge size becomes small? *We show that the answer depends on whether the liquid energetically spreads at the solid–solid interface and, in either case, the minimization of total free energy suggests that the system adopts the maximum adhesion possible. Specifically, when the liquid spreads, the system asymptotically exhibits capillary adhesion; otherwise, dry adhesion eventually prevails. Naturally, the term "small" for the liquid bridge should be defined relative to the characteristic size of the specific system. We then elucidate the capillary and dry adhesion interplay by examining two representative systems: the adhesion of a folded elastica loop and the adhesion of a rigid sphere on a linearly elastic half-space. The corresponding small parameters are defined by a combination of geometry and elasticity. In particular, in the second system, we demonstrate the emergence of modified Johnson–Kendall–Roberts and Derjaguin–Muller–Toporov limits in systems of both dry and capillary adhesion, with a continuous transition governed by an effective liquid volume that we define.*
[DOI: 10.1115/1.4069116]

Keywords: capillary adhesion, liquid bridge, elastica, elastocapillarity, meniscus, elasticity, energy release rate and delamination, failure criteria

1 Introduction

In confined spaces or at lines of contact between solid surfaces, vapor condensation may lead to the formation of liquid bridges [1,2]. For hydrophilic surfaces, these bridges exhibit a negative Laplace pressure (relative to the atmosphere) and generate attractive forces that "glue" the surfaces together—a phenomenon known as capillary adhesion [2,3]. Capillary adhesion plays a crucial role in a diverse range of natural and engineered settings. It enables insects to climb vertical surfaces [4,5], influences the deformation and strength of granular materials [6,7], and contributes to the coalescence of paintbrush hairs upon withdrawal from water for drawing fine lines [8,9]. Furthermore, capillary adhesion underlies stiction in micro- and nanoelectromechanical systems [10–12], the pull-off forces measured in atomic force microscopy or nanoindentation tests [13–16], the capillary transfer of electronic membranes and two-dimensional crystals [17–19], and the self-assembly during the drying of pre-wetted nanowires, forests, and foils [20–24], among many other applications.

Capillary adhesion shares a number of conceptual similarities with dry adhesion, even though the latter originates from an entirely different mechanism, which is based on direct surface–surface intermolecular interactions (e.g., van der Waals forces) [25–27]. A particular example is that both mechanisms would lead to a finite pull-off force required to separate a sphere from a flat surface (Fig. 1(*a*)). In the case where both the sphere and the surface are rigid, Derjaguin [28] discussed the liquid-bridge effect, and McFarlane and Tabor [29] further verified that this pull-off force is given by

$$F_{\text{wet}} = 4\pi R_{\text{s}}\gamma\cos\theta \tag{1.1}$$

where γ denotes the surface tension of the liquid and θ is the contact angle on both the sphere and the flat surface (assuming they are identical). Equation (1.1) is valid when the size of the liquid bridge is small compared to the sphere radius (i.e., $\ell_{\text{m}} \ll R_{\text{s}}$ in Fig. 1(*a*)) [28,29]. In contrast, in the absence of a liquid bridge, Bradley showed that intermolecular interactions between the sphere and the flat surface result in a net adhesive force

$$F_{\text{dry}} = 2\pi R_{\text{s}}\Gamma \tag{1.2}$$

where Γ represents the work of adhesion (i.e., the energy required to separate the two surfaces per unit area from equilibrium spacing z_0

[1]Corresponding author.

Contributed by the Applied Mechanics Division of ASME for publication in the Journal of Applied Mechanics. Manuscript received May 11, 2025; final manuscript received June 30, 2025; published online July 23, 2025. Assoc. Editor: Ruike Renee Zhao.

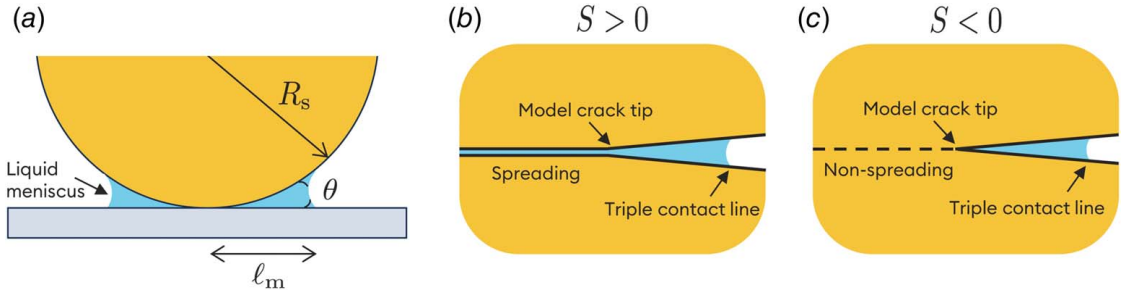

Fig. 1 (*a*) Adhesion between a sphere of radius R_s and a flat surface in the presence of a liquid meniscus. θ denotes the water contact angle (assuming the same for the sphere and the flat surface); (*b*) schematic of a system with a positive spreading parameter as defined in Eq. (2.1). In this case, the liquid spreads so that no effective solid–solid contact exists across the entire interface; (*c*) schematic of a system with a negative spreading parameter. In this case, the interface can be divided into three regions: a solid–solid contact region, a liquid meniscus region, and a solid–vapor region.

to infinity in a vapor medium) [30]. Subsequent studies have demonstrated that Eq. (1.2) is independent of the specific interfacial traction-separation laws, provided that the sphere is sufficiently rigid and large ($R_s \gg z_0$) [25,31]. Comparing Eqs. (1.1) and (1.2) suggests that, in the sense of pull-off force, the liquid bridge contributes an effective adhesion energy of

$$\Gamma_{wet} = 2\gamma \cos\theta \tag{1.3}$$

This then raises an important question: *which mechanism—capillary or dry adhesion—will take over the overall adhesion of the system as the liquid evaporates or ℓ_m decreases?*

The question just posed may initially seem paradoxical, as it involves reconciling two distinct adhesion mechanisms. And a trivial answer can be immediately given: when the size of the liquid bridge (characterized by ℓ_m) falls below the microscopic length scale of intermolecular interactions (say z_0), the physical picture requires that the effective adhesion is eventually controlled by dry adhesion, i.e.,

$$\Gamma_{eff} \to \Gamma \tag{1.4}$$

as $\ell_m \ll z_0$. Before reaching this extreme, however, the system will experience a considerable regime in which $z_0 \ll \ell_m \ll R_s$ as the liquid volume decreases, because of the markedly different interacting ranges of capillary forces and intermolecular forces. Within this intermediate regime, the overall adhesion should result from a combination of capillary and solid–solid dry adhesion mechanisms [32]. The effective adhesion Γ_{eff} in this context is not immediately clear [33–36], to the best of our knowledge. In this work, we will apply an energetic argument to show that the combination of capillary and dry adhesion leads the system to asymptotically adopt the maximum possible adhesion, namely

$$\Gamma_{eff} \to \max\{2\gamma\cos\theta,\ \Gamma\} \tag{1.5}$$

both in the rigid limit and in the alternative flexible limit, where elastic deformation of the surfaces must be taken into account.

2 The Spreading Parameter

We first discuss the energetic difference between dry adhesion and the effective capillary adhesion given in Eq. (1.3). Specifically, it is natural to define the difference of the two by

$$S = 2\gamma\cos\theta - \Gamma \tag{2.1}$$

Recalling Young's equation, $\gamma_{sl} = \gamma_{sv} - \gamma\cos\theta$ and Dupré's equation, $\Gamma = 2\gamma_{sv} - \gamma_{ss}$ [2,3,37], Eq. (2.1) can be rewritten as

$$S = \gamma_{ss} - 2\gamma_{sl} \tag{2.2}$$

where γ_{ij} denotes the interfacial energy density between phases i and j, with the subscripts s, l, and v representing solid, liquid, and vapor, respectively. S in this form is often termed spreading parameter [37]. Physically, it characterizes the energy released when the liquid spreads along the solid–solid interface, as this process involves the loss of solid–solid interfacial energy and the gain of two solid–liquid interfacial energies [37]. If S is positive, indicating a net energy release, the liquid will spread energetically (see schematic in Fig. 1(*b*)); otherwise, the liquid will not spread, and solid–solid contact will persist (see Fig. 1(*c*)).

The distinction between spreading and non-spreading lies in whether the solid–solid interaction across the liquid medium should be considered in the overall effective adhesion. This is important because the adhesive force due to dry adhesion in Eq. (1.2) must be modified at least, while the adhesive force due to capillary adhesion in Eq. (1.1) remains valid. In the spreading case ($2\gamma\cos\theta > \Gamma$), the liquid spontaneously infiltrates the solid–solid interface, eliminating solid–solid adhesion so that the effective adhesion is solely provided by capillary forces, i.e.,

$$\Gamma_{eff} = 2\gamma\cos\theta \quad \text{for} \quad S > 0 \tag{2.3}$$

In the non-spreading case ($2\gamma\cos\theta < \Gamma$), solid–solid contact is well established; however, the parameter Γ in Eq. (1.2) should be replaced by $2\gamma_{sl} - \gamma_{ss}$, since this quantity now represents the energy required to separate the two solid surfaces from equilibrium to infinity in the liquid medium. Consequently, the combined effects of dry and capillary adhesion yield

$$\Gamma_{eff} = 2\gamma_{sl} - \gamma_{ss} + 2\gamma\cos\theta = \Gamma \qquad \text{for} \quad S < 0 \tag{2.4}$$

which is the dry solid–solid adhesion measured in the vapor medium. Therefore, although dry adhesion and capillary adhesion arise from different mechanisms, the simple energetic analysis indicates that the system ultimately adopts the maximum possible adhesion, with the effective values determined by the sign of the spreading parameter, supporting our claim in Eq. (1.5).

Indeed, this result can be readily understood using a steady-state fracture-mechanics picture (Figs. 1(*b*) and 1(*c*)). In the spreading case (Fig. 1(*b*)), a model crack advancing at a steady-state converts two solid–liquid interfaces into two solid–vapor interfaces. By Young's law, the net energy release per unit crack advance is $2\gamma_{sv} - 2\gamma_{sl} = 2\gamma\cos\theta$. In the non-spreading case (Fig. 1(*c*)), the same advance instead gains two solid–vapor interfaces and loses one solid–solid interface, so the required driving energy is $2\gamma_{sv} - \gamma_{ss} = \Gamma$.

In practice, this steady-state picture holds only when the liquid meniscus is small compared to the system's characteristic length —an assumption that becomes subtle for deformable solids. We then turn our attention to relatively compliant substrates, where elasticity cannot be ignored. Two model problems are studied: (i) slender beams made of stiff material, whose compliance arises

from bending, and (ii) bulk elastic slabs that are intrinsically soft. Our central result is that Eq. (1.5) continues to govern the effective adhesion in the limit of a vanishingly small meniscus. Crucially, however, the meaning of "small" now depends on both the geometry and the elasticity of the solids.

3 Problem I: Adhesion of a Folded Elastica Loop

We begin by discussing an Euler elastica folded into a "racket-shaped" loop configuration, maintained by a small liquid meniscus at the self-contacting tail (see Fig. 2). This configuration was first demonstrated and investigated by Py et al. [38], who assumed that the presence of the meniscus effectively produces an adhesion energy of $\Gamma_{\text{eff}} = 2\gamma\cos\theta$ at the contact point. In this context, the theoretical framework is equivalent to the dry adhesion of an elastica loop, as discussed in Refs. [39–44]. Alternatively, a similar (linearized) geometry was examined by Kim and Mahadevan [8], in which capillary adhesion is modeled via the negative Laplace pressure acting within the finite meniscus region. More recently, it has been demonstrated for thin polymer films and two-dimensional crystals that both capillary adhesion and solid–solid interactions across the liquid medium play significant roles in determining the equilibrium configuration [45–49]; a proper utilization of these mechanisms has even facilitated the design of small-scale switches [50]. We then extend the analysis of the self-folding elastica loop by considering the combined effects of dry and capillary adhesion.

3.1 Problem Description. Given the symmetry of the elastica, we focus our analysis on one half (see detailed notations in Fig. 2). To the left of the contact point O (i.e., the model crack tip), the two ends of the elastica are folded together with zero displacement in the y-direction. The elastica is subject to a Laplace pressure within the liquid meniscus region, which extends from O to A, while experiencing a concentrated line force γ originating from surface tension. We take the arc length s as the independent variable (with $s = 0$ at O) and denote the inclination angle by $\phi(s)$, so that the curvature is given by $\kappa(s) = \mathrm{d}\phi/\mathrm{d}s$. The Euler elastica equations, including the lateral pressure $p(s)$, are then given by

$$\frac{\mathrm{d}t}{\mathrm{d}s} - \kappa q = 0, \quad \frac{\mathrm{d}q}{\mathrm{d}s} + \kappa t - p = 0, \quad \text{and} \quad \frac{\mathrm{d}m}{\mathrm{d}s} + q = 0 \tag{3.1}$$

where t, q, and m represent the axial tension, shear force, and bending moment, respectively.

Let the vertical position of the loop at A (i.e., $s = s_{\text{A}}$) be y_{A}. The radius of curvature of the meniscus is given by $r = y_{\text{A}}/\cos(\phi+\theta)$, which leads to a Laplace pressure of $p = \gamma/r = \gamma\cos(\phi+\theta)/y_{\text{A}}$, valid in the interval $0 < s < s_{\text{A}}$. We then express the lateral pressure

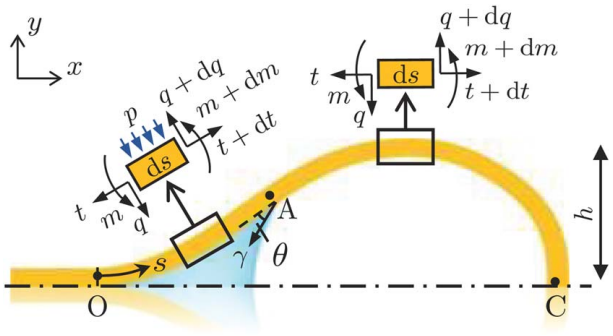

Fig. 2 Adhesion of an Euler elastica. The combined effects of dry and capillary adhesion are characterized by three key contributions: (*i*) a distributed Laplace pressure acting from the model crack tip *O* to the triple contact point *A*, (*ii*) a line force at *A*, and (*iii*) a possible curvature jump at *O* (for the non-spreading case in which there is nontrivial solid–solid adhesion across the liquid medium).

as

$$p = \mathrm{H}_0(s_{\text{A}} - s)\gamma\cos(\phi+\theta)/y_{\text{A}} + \mathrm{H}_{-1}(s - s_{\text{A}})\gamma\sin\theta \tag{3.2}$$

where H_0 is the Heaviside step function and H_{-1} is the Dirac delta function to account for the component of the line force normal to the elastica. We adopt a simple linear constitutive law

$$m = B\kappa \tag{3.3}$$

where B is the bending stiffness per unit length of the elastic loop perpendicular to the plane. Following the formulation presented by Mora et al. [51], we combine Eqs. (3.1) and (3.3) to obtain

$$B\kappa\frac{\mathrm{d}\kappa}{\mathrm{d}s} + \frac{\mathrm{d}t}{\mathrm{d}s} = 0 \tag{3.4}$$

which can be integrated once to yield

$$\mu = \frac{1}{2}B\kappa^2 + t \tag{3.5}$$

where the integration constant μ exhibits a jump at $s = s_{\text{A}}$ due to the component of the line force tangential to the elastica. Combining Eqs. (3.1), (3.3), and (3.5) leads to the final governing equation

$$\frac{\mathrm{d}^2\kappa}{\mathrm{d}s^2} + \frac{1}{2}\kappa^3 - \frac{\mu}{B}\kappa + \frac{p}{B} = 0 \tag{3.6}$$

Let y_{O}, ϕ_{O}, and κ_{O} denote the y-direction displacement, inclination angle, and curvature of the elastica loop at the model crack tip O. Naturally

$$y_{\text{O}} = \phi_{\text{O}} = 0 \tag{3.7}$$

We employ the J-integral to evaluate the energy release rate near the model crack tip O [52]

$$J = 2\times\frac{1}{2}B\kappa_{\text{O}}^2 \tag{3.8}$$

In the spreading case ($S = 2\gamma\cos\theta - \Gamma > 0$), there is no phase change across the crack tip, so $J = 0$. In the non-spreading case ($S < 0$), a finite J is required to supply the energy for the phase change, i.e., $2\gamma_{\text{sl}} - \gamma_{\text{ss}} = -S$. Using Eqs. (2.1) and (3.8), we obtain the boundary condition

$$\kappa_{\text{O}} = \sqrt{\mathrm{H}_1(\Gamma - 2\gamma\cos\theta)/B} \tag{3.9}$$

where H_1 is the half-range function defined as $\mathrm{H}_1(x) = x$ for $x > 0$ and $\mathrm{H}_1(x) = 0$ for $x \le 0$.

In addition, the overall force balance indicates that the axial tension prior to the crack tip is zero and remains continuous across the crack tip (i.e., $\mu = \frac{1}{2}B\kappa_{\text{O}}^2$ for $s < s_{\text{A}}$). Across the triple contact line at $s = s_{\text{A}}$, the line force due to surface tension produces a jump in tension of $\gamma\cos\theta$. We can then express the integration constant μ as

$$\mu = \frac{1}{2}\mathrm{H}_1(\Gamma - 2\gamma\cos\theta) + \gamma\cos\theta\,\mathrm{H}_0(s - s_{\text{A}}) \tag{3.10}$$

Lastly, the symmetry conditions for the y-direction displacement and the rotation angle of the loop at point C are given by

$$y_{\text{C}} = 0 \quad \text{and} \quad \phi_{\text{C}} = -\pi/2 \tag{3.11}$$

respectively. This setting, therefore, differs from that in Kim and Mahadevan [8], where only the Laplace pressure is considered (analogous to the Maugis adhesion model [31]), and from that in Py et al. [38], where the effect of the Laplace pressure over a small region is replaced by a jump in κ_{O} corresponding to an effective adhesion of $2\gamma\cos\theta$ (similar to the Johnson–Kendall–Roberts (JKR) adhesion model [53]).

3.2 Nondimensionalization. It is natural to choose the bendo-capillary or bendoadhesive length to rescale the system [11,38,54].

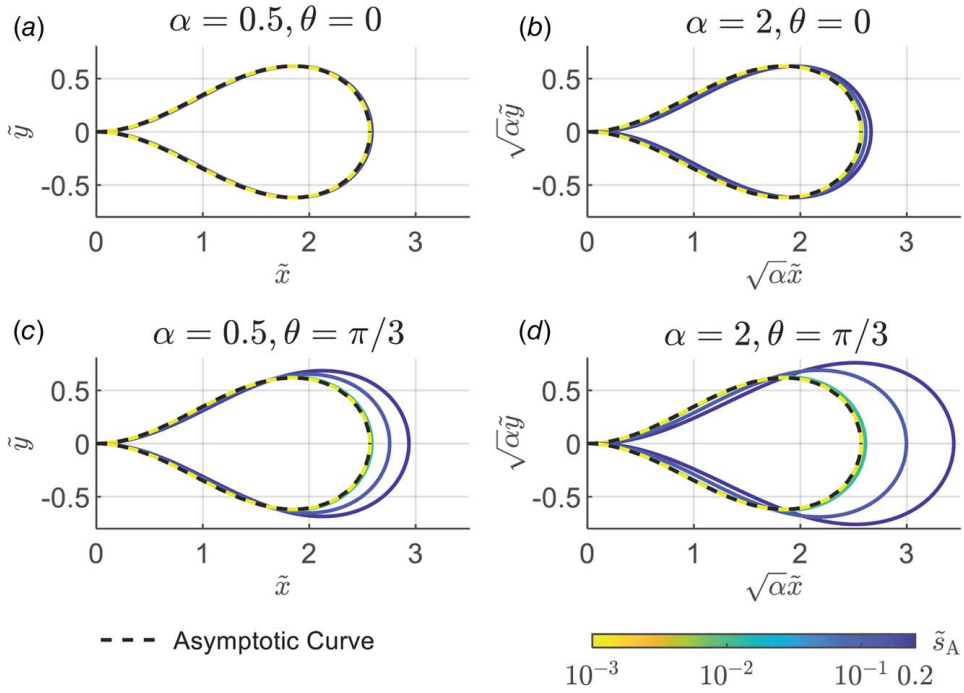

Fig. 3 The shape of a self-adhering elastica loop: (*a*) and (*b*) rescaled shape by $\ell_{ba} = (B/\Gamma)^{1/2}$ for non-spreading systems ($S < 0$ or $\alpha < 1$). The contact angle is 0 in (*a*) and $\pi/3$ in (*b*); (c) and (*d*) rescaled shape by the bendocapillary length $\ell_{bc} = (B/2\gamma\cos\theta)^{1/2} = \ell_{ba}/\sqrt{\alpha}$ defined in Eq. (3.12) for spreading systems ($S > 0$ or $\alpha > 1$). The contact angle is 0 in (*c*) and $\pi/3$ in (*d*). All solid curves are numerically calculated with a specified size of liquid meniscus $\tilde{s}_A$ with values encoded in the color bar. All dashed curves are the same, solved based on Eq. (3.19) with an effective adhesion in Eq. (1.5). (Color version online.)

Here, we choose dry adhesion as the reference and define the bendoadhesive length as

$$\ell_{ba} = \left(B/\Gamma\right)^{1/2} \tag{3.12}$$

In addition, we introduce the parameter comparing capillary adhesion to dry adhesion

$$\alpha = 2\gamma\cos\theta/\Gamma \tag{3.13}$$

We then apply the following nondimensionalization:

$$\tilde{s} = s/\ell_{ba}, \quad \tilde{y} = y/\ell_{ba}, \quad \tilde{\kappa} = \kappa\,\ell_{ba}, \quad \tilde{\mu} = \mu/\Gamma, \quad \text{and} \quad \tilde{p} = pB^{1/2}/\Gamma^{3/2} \tag{3.14}$$

The problem now becomes

$$\frac{\mathrm{d}^2\tilde{\kappa}}{\mathrm{d}\tilde{s}^2} + \frac{1}{2}\tilde{\kappa}^3 - \tilde{\mu}\,\tilde{\kappa} + \tilde{p} = 0 \tag{3.15}$$

where

$$\tilde{\mu} = \frac{1}{2}\,\mathrm{H}_1(1-\alpha) + \frac{1}{2}\,\alpha\,\mathrm{H}_0(\tilde{s} - \tilde{s}_A) \tag{3.16}$$

and

$$\tilde{p} = \alpha\cos(\phi + \theta)\,\mathrm{H}_0(\tilde{s}_A - \tilde{s})/\left(2\tilde{y}_A\cos\theta\right) \tag{3.17}$$

subject to the boundary conditions

$$\tilde{y}_O = 0, \quad \phi_O = 0, \quad \tilde{\kappa}_O = \sqrt{\mathrm{H}_1(1-\alpha)}, \quad \tilde{y}_C = 0, \quad \text{and} \quad \phi_C = -\pi/2 \tag{3.18}$$

Note that the position of the triple contact line is often unknown in practice, as it is typically determined as part of the solution to satisfy the conservation of liquid volume or the equilibrium of chemical potential [35]. However, in this problem, we prescribe $\tilde{s}_A$, so the primary focus is on the combined effects of dry and wet adhesion (although we will consider volume conservation in the model problem discussed in the next section).

The problem specified in Eqs. (3.15)–(3.18) can be viewed as a second-order ordinary differential equation (ODE) in terms of $\tilde{\kappa}$, which is equivalent to a fourth-order ODE in terms of $\tilde{y}$ (since $\mathrm{d}\tilde{y}/\mathrm{d}\tilde{s} = \sin\phi$ and $\mathrm{d}\theta/\mathrm{d}\tilde{s} = \tilde{\kappa}$). Additionally, the arc length from O to C is not known a priori. Thus, a total of five boundary conditions are required, as given in Eq. (3.18). We solve this numerically and obtain the shape of the loop by $\mathrm{d}\tilde{x}/\mathrm{d}\tilde{s} = \cos\phi$ and $\mathrm{d}\tilde{y}/\mathrm{d}\tilde{s} = \sin\phi$.

3.3 Numerical Results. Under a prescribed $\tilde{s}_A$, the problem defined by Eqs. (3.15)–(3.18) is governed solely by the parameter α (defined in Eq. (3.13)) and the contact angle θ (see Fig. 2). We solve this problem numerically using a combination of finite difference and shooting method, thereby transforming the boundary-value problem into an initial value problem. An initial guess for $\mathrm{d}\tilde{x}/\mathrm{d}\tilde{s}$ and $\tilde{s}_C$ is used to solve the equations and obtain the boundary values at $\tilde{s} = \tilde{s}_C$. These computed values are then compared with the prescribed boundary conditions in Eq. (3.18), and Newton's method is employed iteratively to adjust the initial guess until the computed boundary values converge to the specified ones.

Figure 3 shows the shape of the adhered elastic loop computed for various combinations of α and contact angle ϕ. All solid curves are obtained using a prescribed size of the liquid meniscus ($\tilde{s}_A$), with its value encoded in the color bar. In the non-spreading case ($\alpha = 0.5$, so $S < 0$ in Figs. 3(*a*) and 3(*b*), the natural length scale is the bendoadhesive length $\ell_{ba} = (B/\Gamma)^{1/2}$. As $\tilde{s}_A \to 0$, the loop shape progressively contracts and eventually converges to a universal profile (dashed curves in Figs. 3(*a*) and 3(*b*)) that is independent of both the contact angle and the meniscus size. Notably, smaller contact angles accelerate the rate at which this convergence

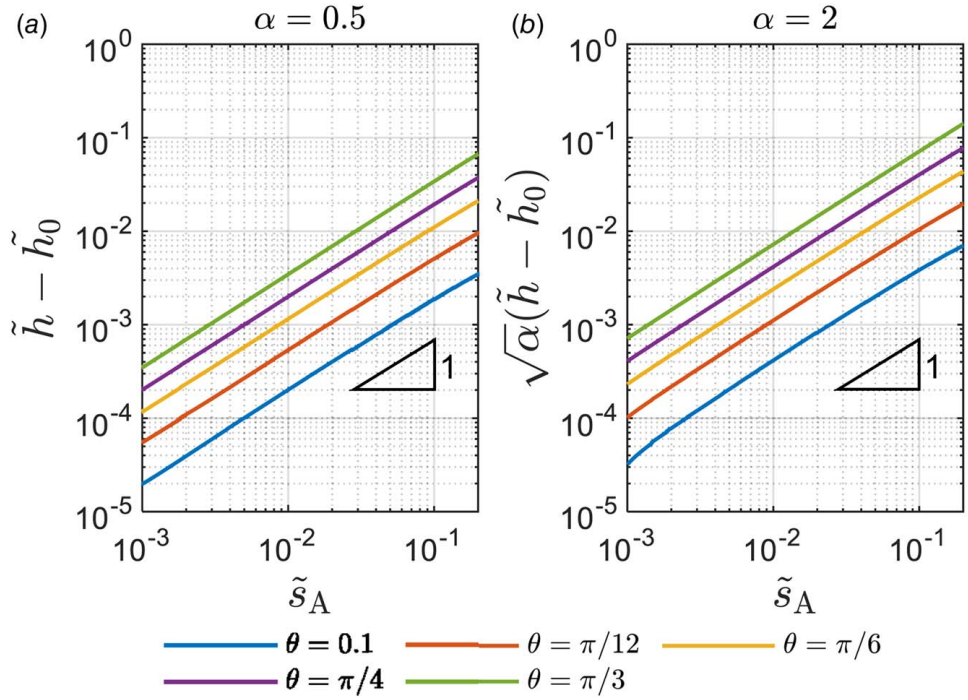

Fig. 4 Rescaled half-width $\tilde{h}$ of the elastica loop as a function of the meniscus size (relative to the limit of $\tilde{s}_A \to 0$, i.e., $\tilde{h}_0$). In both (*a*) the non-spreading case and (*b*) the spreading case, $\tilde{h} - \tilde{h}_0$ is linearly proportional to $\tilde{s}_A$.

occurs. For the spreading case ($\alpha = 2$, so $S > 0$ Figs. 3(*c*) and 3(*d*)), the relevant length scale becomes the bendocapillary length $\ell_{ec} = (B/2\gamma\cos\theta)^{1/2} = \sqrt{\alpha}\,\ell_{ba}$, since the dry-adhesion contribution vanishes. Rescaling the loop by the factor $\sqrt{\alpha}$ then reveals a similar convergence behavior as $\tilde{s}_A \to 0$, yielding an α- and θ-independent profile that is identical to the non-spreading case.

Such an observation of the converged loop shape as $\tilde{s}_A \to 0$ is analogous to the small-scale yielding concept in fracture mechanics [37]. Moreover, the independence of the converged shape on α and θ implies that the system's behavior is governed solely by the effective adhesion energy $\Gamma_{eff} = \max\{2\gamma\cos\theta, \Gamma\}$ (see Eq. (1.5)), rather than by the specific adhesion mechanism. We next derive this asymptotic profile by invoking the energy argument, without explicitly integrating the attractive force over a finite region. Specifically, in the limit $\tilde{s}_A \to 0$, the domain of nonzero Laplace pressure shrinks to zero and the triple-line point A merges with the model crack tip O. As such, the governing Eq. (3.6) reduces to

$$\frac{d^2\tilde{\kappa}}{d\tilde{s}^2} + \frac{1}{2}\tilde{\kappa}^3 - \tilde{\mu}\tilde{\kappa} = 0 \tag{3.19}$$

Combining the effective adhesion Γ_{eff} and the energy release rate evaluated by the J-integral in Eq. (3.8) leads to the critical curvature at the model crack tip

$$\kappa_O = \sqrt{\max\{2\gamma\cos\theta,\ \Gamma\}/B} \tag{3.20}$$

which gives the dimensionless integral constant $\tilde{\mu} = \frac{1}{2}H_1(1-\alpha) + \frac{1}{2}\alpha$. The boundary conditions in this limit reduce to

$$\tilde{y}_O = 0, \quad \phi_O = 0, \quad \tilde{\kappa}_O = \sqrt{H_1(1-\alpha)+\alpha}, \quad \tilde{y}_C = 0, \quad \text{and} \quad \phi_C = -\pi/2 \tag{3.21}$$

We present the numerically calculated results based on the reduced problem in Eqs. (3.19)–(3.21) in Fig. 3 (dashed curves), finding a consistent transition from the perspective of capillary force to the energy perspective as the liquid meniscus vanishes.

In Fig. 4, we further examine how the shape of the elastica loop converges to the asymptotic curve. Specifically, we consider the loop's half-width h (see Fig. 2) and measure its deviation from the limiting value h_0 as $\tilde{s}_A \to 0$. Our numerical simulations yield $h_0 \approx 0.437$, consistent with the result reported by Py et al. [38]. We find that the difference $\tilde{h} - \tilde{h}_0$ scales linearly with $\tilde{s}_A$ (with slopes of unity in log-log plot in Fig. 4), while the contact angle θ influences only the rate of convergence.

This linear relation could be readily understood via a scaling argument. In the limit $\tilde{s}_A \ll 1$, we have $\tilde{m} \sim \mathcal{O}(1)$, $\tilde{\kappa} \sim \tilde{m}$, $\theta \sim \tilde{\kappa}\tilde{s} \sim \mathcal{O}(\tilde{s}_A)$, and $\tilde{y} \sim \tilde{\theta}\tilde{s} \sim \mathcal{O}(\tilde{s}_A^2)$ within the Laplace-pressure region $(0, \tilde{s}_A)$. Equation (3.15) can then be linearized by omitting high-order terms, yielding the quartic-polynomial solution

$$\tilde{y} = \frac{1}{2}\tilde{\kappa}_O\tilde{s}^2 + \frac{1}{6}\tilde{q}_O\tilde{s}^3 - \frac{1}{24}\tilde{p}\tilde{s}^4 + \mathcal{O}(\tilde{s}_A^4) \tag{3.22}$$

where $\tilde{\kappa}_O$ is the curvature, $\tilde{q}_O$ is the dimensionless shear force at point O, and $\tilde{p}$ is the Laplace pressure with condition: Eq. (3.17) $2\tilde{p}\tilde{y}_A = \alpha\cos(\phi_A + \theta)/\cos\theta = \alpha + \mathcal{O}(\tilde{s}_A)$. The y-direction force equilibrium gives $\tilde{q}_O\tilde{s}_A = \tilde{p}\tilde{s}_A^2 + \tilde{q}_A\tilde{s}_A + 2\alpha\sin(\phi_A + \theta)\tilde{s}_A/\cos\theta$, where the shear force at point A follows $\tilde{q}_A = \tilde{m}_C/(\tilde{x}_C - \tilde{x}_A) \sim \mathcal{O}(1)$ according to the moment of equilibrium from point A to point C. Combining these equations, we obtain $\tilde{q}_O\tilde{s}_A = \tilde{p}\tilde{s}_A^2 + \mathcal{O}(\tilde{s}_A) = 2\sqrt{H_1(1-\alpha)+\alpha} - 2\sqrt{H_1(1-\alpha)} + \mathcal{O}(\tilde{s}_A)$. We then arrive at the curvature of the loop at the triple contact line

$$\tilde{\kappa}_A = \tilde{\kappa}_O + \tilde{q}_O\tilde{s}_A - \frac{1}{2}\tilde{p}\tilde{s}_A^2 + \mathcal{O}(\tilde{s}_A^2) = \sqrt{H_1(1-\alpha)+\alpha} + \mathcal{O}(\tilde{s}_A) \tag{3.23}$$

which not only justifies the effective adhesion Γ_{eff}, but also clarifies the order-$\tilde{s}_A$ correction to the loop geometry when the finite meniscus size is considered.

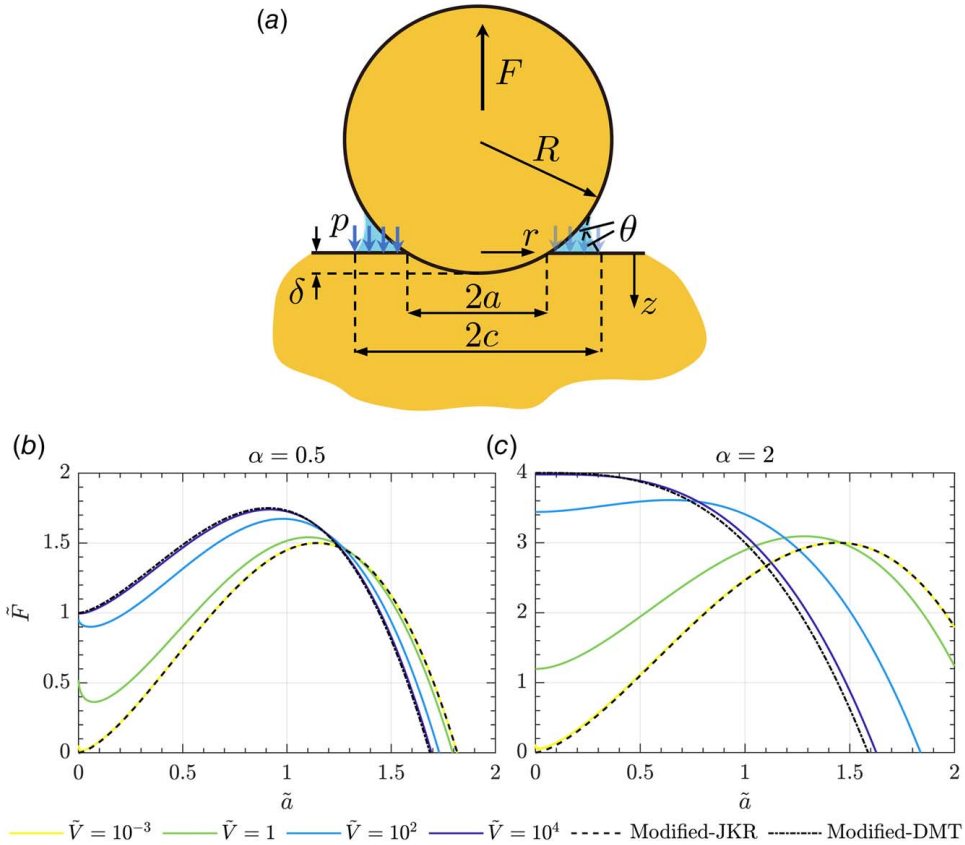

Fig. 5 Adhesion of a rigid sphere on an elastic substrate in the presence of a liquid meniscus: (*a*) schematic of a sphere indenting the substrate with a depth of δ, forming a contact area of radius *a* and a circular crack front at $r = a$. An annular liquid film exerts a Laplace pressure in the wet region $a < r < c$; (*b*), (*c*) relationship between the rescaled pulling force ($\tilde{F}$) and contact radius ($\tilde{a}$) in the non-spreading case (*b*) and the spreading case (*c*). For a prescribed dimensionless liquid volume $\tilde{V}$, the adhesion force is computed numerically from Eqs. (4.14) and (4.16). As $\tilde{V} \to 0$, all curves recover the modified JKR limit (dashed curves, given by Eq. (4.18)); as $\tilde{V} \to \infty$, they approach the modified DMT limit (dash-dotted curves, given by Eq. (4.22)).

4 Problem II: Adhesion of a Rigid Sphere on an Elastic Substrate

We now extend the concept of the effective work of adhesion, Γ_{eff}, to the canonical problem of a rigid sphere adhering to an elastic substrate in the presence of a liquid meniscus (see schematic in Fig. 5(*a*)). Such a configuration has long served to elucidate dry adhesion mechanics in elastic contacts [26,31,53,55]. Two particular examples can be given by the JKR theory (valid for large, compliant spheres with strong surface energy) [53] and the Derjaguin–Muller–Toporov (DMT) theory (applicable to small, relatively rigid spheres with weak adhesion) [55]. Subsequent studies by Maugis [34], Fogden and White [35], and Goryacheva and Makhovskaya [56] (as well as others [57,58]) incorporated capillary forces but neglected solid–solid adhesion. Notably, the concepts of JKR and DMT theory have now been extended to a range of configurations, including graded elastic materials [59,60], thin membranes [16,27], and shells [61,62]. Recently, Salez et al. have further included the effect of solid surface tension, which could give rise to a Young–Dupré limit [63]. More recently, Qian et al. [32] employed Maugis's framework [37] to treat dry and wet adhesion simultaneously, accounting for meniscus curvature, substrate deformation, and sphere geometry. However, their results did not recover the JKR or DMT limits—likely because the thermodynamic distinction between the combined and single-mode adhesion was not clearly defined, nor was a physical transition parameter introduced [32]. Building on these insights, we here incorporate both capillary and dry adhesion into a unified framework (similar to Problem I). We will show that in this setting, the effective size of the liquid meniscus depends on the adhesion, sphere radius, and the elasticity of the substrate in a complex manner. We will also show that the adhesion behavior indeed can transition from a JKR-type limit to a DMT-type limit as the effective size of the liquid meniscus increases.

4.1 Problem Description. As shown in Fig. 5(*a*), a rigid sphere of radius R_s is in adhesive, frictionless contact with an elastic half-space whose plane-strain modulus is defined by $E^* = E/(1-\nu^2)$, where E and ν denote the substrate's Young's modulus and Poisson's ratio, respectively. The contact region is within a circle of radius a, surrounded by a liquid bridge forming an annulus between $r = a$ and $r = c$. The sphere indents the substrate by a depth δ, and the applied load F balances the combined capillary and dry adhesion forces and elastic forces. In the contact area (i.e., $0 \le r \le a$), the sphere and the deformed substrate share the same profile in the z-direction, which can be approximated by $f(r) = -r^2/(2R_s)$. Outside the contact area (i.e., $r > a$), the z-direction stress is given by a piecewise function, which equals the Laplace pressure P in the wet region and become zero outside the liquid meniscus. With no-shear conditions, the problem can be specified as follows:

$$\begin{cases} u_z(r,0) = \delta + f(r), & 0 \le r \le a \\ \sigma_z(r,0) = -P\,\mathrm{H}_0(c-r), & r > a \\ \tau_{rz}(r,0) = 0, & r > 0 \end{cases} \tag{4.1}$$

The boundary-value problem in Eq. (4.1) was addressed by Butler [64], who—while neglecting solid–solid dry adhesion—introduced a biharmonic Love stress function and applied the Hankel transform to reduce the mixed boundary conditions to a system of dual integral equations in Bessel kernels, following the method discussed in Refs. [65–67]. Here, we follow Butler's solution strategy but restore the omitted inverse-square-root stress singularity at the model crack tip ($r = a$). Specifically, defining $\rho = r/a$, $m = c/a$, Butler showed that the separation outside the contact region ($\rho > 1$), the normal stress inside the contact region ($\rho < 1$), and the applied pulling force can be expressed respectively as

$$h(a\rho) = \frac{a^2}{\pi R_s}\left[\sqrt{\rho^2-1} + (\rho^2-2)\arctan\sqrt{\rho^2-1}\right] - \frac{2a}{\pi}\left(\frac{\delta}{a} - \frac{a}{R_s}\right)\arctan\sqrt{\rho^2-1} + \frac{4aP}{\pi E^*}\int_1^{\min\{\rho,m\}}\sqrt{\frac{m^2-\rho^2}{\rho^2-u^2}}\,\mathrm{d}u \tag{4.2}$$

$$\sigma(a\rho) = \frac{2E^*a}{\pi R_s}\sqrt{1-\rho^2} + \frac{E^*}{\pi}\left(\frac{\delta}{a} - \frac{a}{R_s} - \frac{2P}{E^*}\sqrt{m^2-1}\right)\frac{1}{\sqrt{1-\rho^2}} + \frac{2P}{\pi}\arctan\sqrt{\frac{m^2-1}{1-\rho^2}} \tag{4.3}$$

and

$$F = -\frac{4E^*a^3}{3R_s} - 2E^*a^2\left(\frac{\delta}{a} - \frac{a}{R_s} - \frac{2P}{E^*}\sqrt{m^2-1}\right) - 2a^2P\left[m^2\arctan\sqrt{m^2-1} + \sqrt{m^2-1}\right] \tag{4.4}$$

The singular term of the stress at the crack tip $r = a$ (i.e., $\rho = 1$) was set to zero by Butler [64]. We accept this singularity of σ. In particular, since the corresponding term is proportional to $(1-\rho^2)^{-1/2}$, we can obtain the stress intensity factor

$$K_I = \sqrt{\frac{a}{\pi}}\left[E^*\left(\frac{a}{R_s} - \frac{\delta}{a}\right) + 2P\sqrt{m^2-1}\right] \tag{4.5}$$

Similar to that in the preceding section, the energy release rate at the model crack tip is not necessarily zero, but instead satisfies

$$\frac{K_I^2}{2E^*} = \max\{\Gamma - 2\gamma\cos\theta,\ 0\} \tag{4.6}$$

where the coefficient $1/2$ is due to the fact that only half of the crack is deformable. Combining Eqs. (4.5) and (4.6) gives a relation between the indentation depth and the contact radius

$$\delta = \frac{a^2}{R_s} + \frac{2aP}{E^*}\sqrt{m^2-1} - \sqrt{2\pi a\max\{\Gamma - 2\gamma\cos\theta,\ 0\}/E^*} \tag{4.7}$$

Under the assumption of small deformations and displacements, the Laplace pressure can be approximated by

$$P = \frac{-2\gamma\cos\theta}{h(am)} \tag{4.8}$$

and the volume of the liquid can then be calculated as

$$V = \frac{a^4}{2R}\left[(m^4-4m^2)\arctan\sqrt{m^2-1} + (2+m^2)\sqrt{m^2-1}\right] + 2a^3\left(\frac{\delta}{a} - \frac{a}{R_s}\right)\left(\sqrt{m^2-1} - m^2\arctan\sqrt{m^2-1}\right) + \frac{8a^3P}{3E^*}(m-1)^2(2m+1) \tag{4.9}$$

4.2 Nondimensionalization. A simple nondimensionalization might take the sphere radius R_s as the characteristic length; however, this accounts only for geometry and neglects both elasticity and adhesion. To capture those effects, we again take the dry adhesion as a reference and introduce the dimensionless elastoadhesion parameter

$$\tau = \left(\frac{3\pi\Gamma}{4E^*R_s}\right)^{1/3} \tag{4.10}$$

which compares the elastoadhesive length Γ/E^* to the sphere radius R_s. We adopt the following nondimensionalization

$$\tilde{a} = \frac{a}{R_s\tau},\ \tilde{r} = \frac{r}{R_s\tau},\ \tilde{h} = \frac{h}{R_s\tau^2},\ \tilde{\delta} = \frac{\delta}{R_s\tau^2},\ \tilde{F} = \frac{F}{\pi R_s\Gamma},\ \tilde{P} = \frac{PR_s\tau^2}{\pi\Gamma} \tag{4.11}$$

and

$$\tilde{V} = \frac{V}{R_s^3\tau^4} = \frac{4^{4/3}E^{*4/3}V}{(3\pi)^{4/3}\Gamma^{4/3}R_s^{5/3}} \tag{4.12}$$

allowing the solutions in Eqs. (4.2)–(4.9) to be independent of τ. In particular, introducing an auxiliary variable $y = \sqrt{m^2-1}$, we have

$$\tilde{P}(\tilde{a}, y) = 3(g_1 + g_3)/(32\,\tilde{a}g_2) \tag{4.13}$$

$$\tilde{F}(\tilde{a}, y) = \sqrt{6\tilde{a}^3\mathrm{H}_1(1-\alpha)} - \tilde{a}^3 - 3\tilde{a}(g_1+g_3)\left[y + (1+y^2)\arctan y\right]/(16\,g_2) \tag{4.14}$$

$$\tilde{\delta}(\tilde{a}, y) = \tilde{a}^2 - \sqrt{8\,\tilde{a}\mathrm{H}_1(1-\alpha)/3} + y(g_1+g_3)/(4\,\tilde{a}g_2) \tag{4.15}$$

$$\tilde{V}(\tilde{a}, y) = 2\tilde{a}^4\left[y(3+y^2) - (3-y^2)(1+y^2)\arctan y\right] - \sqrt{192\,\tilde{a}^5\mathrm{H}_1(1-\alpha)/9}\times\left[y - (1+y^2)\arctan y\right] + \left[4\,(1+y^2)^{3/2} - (4+3\,y^2) - 3\,y(1+y^2)\arctan y\right] \times (g_1+g_3)/(6\,g_2) \tag{4.16}$$

where

$$\begin{aligned} g_1(\tilde{a}, y) &= \tilde{a}^2\left[(1-y^2)\arctan y - y\right] - \arctan y\sqrt{32\,\tilde{a}\mathrm{H}_1(1-\alpha)/3} \\ g_2(\tilde{a}, y) &= \sqrt{1+y^2} - 1 - y\arctan y \\ g_3(\tilde{a}, y) &= \sqrt{\left[\arctan y\sqrt{32\,\tilde{a}\mathrm{H}_1(1-\alpha)/3} + \tilde{a}^2\left(y + (y^2-1)\arctan y\right)\right]^2 - 64\,\alpha\tilde{a}g_2/3} \end{aligned} \tag{4.17}$$

Remarkably, Eqs. (4.13)–(4.17) suggest that with a given α, all quantities can be exclusively expressed as functions of the dimensionless contact radius $\tilde{a}$ and the geometric quantity y, independent of any other variables. In practice, we prescribe the rescaled

liquid volume $\tilde{V}$ and then calculate the corresponding y as well as the required pulling force and the indentation depth for various contact radius $\tilde{a}$, as partially shown in Figs. 5(*b*) and 5(*c*). Interestingly, in both the non-spreading case ($\alpha < 1$ in Fig. 5(*b*)) and the spreading case ($\alpha > 1$ in Fig. 5(*c*)), the $\tilde{F}$–$\tilde{a}$ curves are found to approach asymptotic curves when $\tilde{V} \ll 1$ or $\tilde{V} \gg 1$, which we discuss in the following.

4.3 Modified Johnson–Kendall–Roberts and Derjaguin–Muller–Toporov Limits. We first discuss the small volume limit, which we term the *modified JKR limit*. Equation (4.16) suggests that $\tilde{V} \to 0$ is equivalent to setting $y \to 0$. We then expand $\tilde{F}$ in Eq. (4.14) at $y = 0$ to obtain

$$\tilde{F} = -\tilde{a}^3 + \sqrt{6\,\tilde{a}^3(\mathrm{H}_1(1-\alpha)+\alpha)} + \mathcal{O}(y^2) \tag{4.18}$$

which gives rise to the dashed curves in Figs. 5(*b*) and 5(*c*). Similarly, the rescaled indentation depth can also be given as a function of the contact radius as $y \to 0$

$$\tilde{\delta} = \tilde{a}^2 - \sqrt{8(\mathrm{H}_1(1-\alpha)+\alpha)/3\tilde{a}} + \sqrt{8\mathrm{H}_1(1-\alpha)/3\tilde{a}} \times (1-\tilde{a}) + \mathcal{O}(y^2) \tag{4.19}$$

Physically, systems with vanishing dimensionless liquid volume, $\tilde{V} \ll 1$, correspond to small τ, i.e., to the regime of large adhesion energy Γ and sphere radius R_s, and small elastic modulus E^*, according to Eq. (4.10). Therefore, in the limit $\tilde{V} \ll 1$, the liquid meniscus is expected to behave like JKR-type adhesion. Unlike classic JKR adhesion, however, when both solid–solid interaction and capillary contributions are included, the effective work of adhesion becomes Γ_{eff}, as defined in Eq. (1.5). This is most clearly seen by examining the pull-off force, i.e., the maximum pulling force in Eq. (4.18)

$$\tilde{F}_{\mathrm{Pull}}\text{-off}^{\mathrm{JKR}} = \frac{3}{2}\mathrm{H}_1(1-\alpha) + \frac{3}{2}\alpha, \quad \text{as} \quad \tilde{V} \ll 1 \tag{4.20}$$

Its dimensional form reads

$$F_{\mathrm{pull}}\text{-off}^{\mathrm{JKR}} = \frac{3}{2}\pi R_s \max\{\Gamma, 2\gamma\cos\theta\} \tag{4.21}$$

Since the classical JKR model predicts a pull-off force of $32\pi R_s\,\Gamma$ for pure dry adhesion [26,53], its JKR-type extension to combined dry and capillary adhesion is obtained simply by replacing Γ with Γ_{eff}, in perfect agreement with the results for elastica discussed in the preceding section.

In contrast to the elastica problem, the adhesive contact of a rigid sphere on an elastic half-space exhibits an alternative asymptote when the dimensionless liquid volume is large ($\tilde{V} \gg 1$; see the dash-dotted curves in Figs. 5(*b*) and 5(*c*)). In this regime, the capillary bridge extends so far beyond the contact zone that its Laplace pressure can be simply considered as acting over an essentially Hertzian contact in the spreading case or modified JKR contact in the non-spreading case. In either case, the additional substrate deformation due to capillarity is negligible. We therefore term this the *modified DMT limit*, since it parallels the classical Derjaguin–Muller–Toporov assumption of unchanged elastic deformation under long-range adhesive stresses [55]. Indeed, as $\tilde{V} \to \infty$, the meniscus radius greatly exceeds the contact radius, so that capillary forces contribute a uniform pull-off stress, just as in the DMT picture of solid–solid adhesion [26,68].

We then expand $\tilde{F}$ in Eq. (4.14) at $y = \infty$ (equivalent to $\tilde{V} \to \infty$)

$$\tilde{F} = 2\alpha - \tilde{a}^3 + \sqrt{6\mathrm{H}_1(1-\alpha)\tilde{a}^3} + \mathcal{O}(1/y) \tag{4.22}$$

giving rise to the dash-dotted curves in Figs. 5(*b*) and 5(*c*). The corresponding indentation depth is given by

$$\tilde{\delta} = \tilde{a}^2 - \sqrt{8\tilde{a}\mathrm{H}_1(1-\alpha)/3} + \mathcal{O}(1/y) \tag{4.23}$$

The pull-off force in the modified DMT limit is found to be

$$\tilde{F}_{\mathrm{Pull}}\text{-off}^{\mathrm{DMT}} = \frac{3}{2}\mathrm{H}_1(1-\alpha) + 2\alpha, \quad \text{as} \quad \tilde{V} \to \infty \tag{4.24}$$

This can be thought of as the combination of the DMT limit of capillary adhesion and the JRK limit of dry adhesion (if the liquid does not spread into the interface). The dimensional form of Eq. (4.24) reads

$$F_{\mathrm{pull}}\text{-off}^{\mathrm{DMT}} = \begin{cases} \frac{3}{2}\pi R_s\Gamma + \pi R_s\gamma\cos\theta & \text{for} \quad \alpha < 1 \\ 4\pi R_s\gamma\cos\theta & \text{for} \quad \alpha > 1 \end{cases} \tag{4.25}$$

Therefore, in the modified DMT limit, the influence of both solid–solid adhesion (through the liquid medium) and capillary adhesion exists in the non-spreading case ($\alpha < 1$). And only the spreading case ($\alpha > 1$) recovers the classical prediction of DMT (with Γ replaced by $2\gamma\cos\theta$).

Notably, the dimensionless liquid volume $\tilde{V}$ defined in Eq. (4.12) plays the role of a Tabor parameter for our system, governing the transition between the modified JKR and modified DMT limits. This transition is further illustrated in Fig. 6, where the pull-off force $\tilde{F}_{\mathrm{pull}}$-off is computed from Eqs. (4.14)–(4.16) as a function of α for several fixed values of $\tilde{V}$. We use three background shadings to distinguish (i) the spreading regime ($\alpha > 1$), (ii) the non-spreading hydrophilic regime ($\alpha < 1, \theta < \pi/2$), and (iii) the non-spreading hydrophobic regime ($\alpha < 1, \theta > \pi/2$). In every regime, the computed pull-off force converges to the modified JKR asymptote as $\tilde{V} \ll 1$ and to the modified DMT asymptote as $\tilde{V} \gg 1$. Interestingly, in the hydrophobic, non-spreading case, the meniscus confined near the contact edge yields a positive Laplace pressure that opposes adhesion and thus reduces the pull-off force below its JKR value (i.e., $F_{\mathrm{pull}}\text{-off} \le F_{\mathrm{pull}}\text{-off}^{\mathrm{JKR}}$).

We emphasize that our entire solution is formulated in dimensionless variables (denoted by tildes). Although one might be tempted to associate $\tilde{V} \ll 1$ or $\tilde{V} \gg 1$ directly with a "small" or "large" liquid volume V relative to the sphere size R_s^3, in fact $\tilde{V} = V/(R_s^3\,\tau^4)$, so that a small $\tilde{V}$ may arise from any combination of (i) a geometrically small liquid volume V, (ii) a strong adhesion (large Γ) relative to elasticity (small E^*), or (iii) both. Likewise, a large $\tilde{V}$ can result from a large V, weak adhesion, and stiff substrate. Moreover, identical values of $\tilde{a}$ or $\tilde{\delta}$ do not necessarily correspond to the geometrically similar deformation, since horizontal lengths are rescaled $R_s\,\tau$ while vertical lengths are rescaled by $R_s\,\tau^2$. Note that the results are based on small deformation and displacement

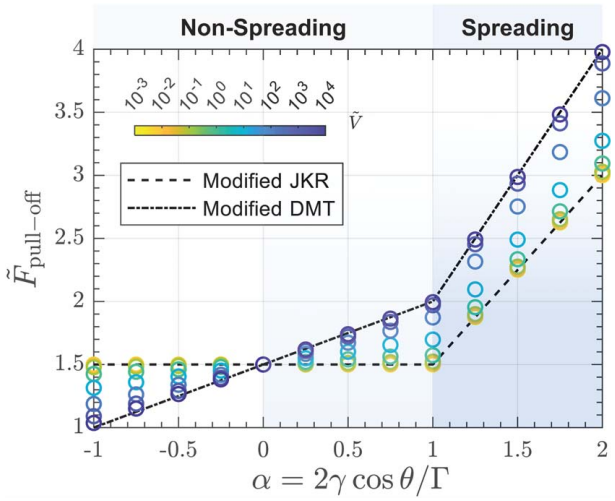

Fig. 6 Dimensionless pull-off force as a function of α under various prescribed $\tilde{V}$. The pull-off force transitions from the modified JKR limit given in Eq. (4.20) at small $\tilde{V}$ to the modified DMT limit given in Eq. (4.24) at large $\tilde{V}$ for arbitrary α.

assumptions so a relatively large τ is required. These considerations underscore that adhesion in soft contacts is governed by a combination of geometry, elasticity, and surface energies. Only by nondimensionalizing with the appropriate combination can one collapse the diverse behaviors (from JKR-type to DMT-type) onto a universal master curve.

5 Conclusion

The present work has established a self-consistent theoretical framework for the interplay of dry and capillary adhesion of elastic structures and solids at an intermediate regime. Specifically, we have discussed in detail the effective adhesion when the size of the liquid bridge is much smaller than the system size while remaining much greater than the microscopic length. By introducing the spreading parameter, we determine the conditions under which a liquid exhibits either spreading or non-spreading behavior. Although these two scenarios are fundamentally distinct, they can be unified within a single theoretical framework by incorporating an energy release rate at the crack tip. Specifically, in the non-spreading scenario, a finite energy release rate is allowed at the crack tip, whereas it vanishes in the spreading scenario. We have shown that as the size of the liquid bridge is sufficiently small, our results converge to those derived from an energy-based perspective (i.e., JKR-type adhesion). For the elastica, the overall effect of capillary forces manifests as a curvature jump, directly corresponding to the surface and interfacial energy jump at the crack tip. In the case of the sphere on an elastic half-space, the effect of capillary forces, together with the solid–solid interaction across the liquid medium, leads to an effective adhesion identical to the solid–solid interaction across the vapor medium. In addition, we have shown a transition between the small and large liquid volume regimes, conceptually similar to the JKR-to-DMT transition.

Acknowledgment

This work was supported by the National Natural Science Foundation of China (Grant Nos. 12372103 and 12432003) and the Natural Science Foundation of Beijing (Grant No. QY24005).

Conflict of Interest

There are no conflicts of interest.

Data Availability Statement

The datasets generated and supporting the findings of this article are obtainable from the corresponding author upon reasonable request.

References

[1] Wang, J., Wu, H., and Wang, F., 2025, "Refined Kelvin Theory for Capillary Condensation Under Extreme Confinement," Phys. Fluids, **37**(3), p. 032011.
[2] Israelachvili, J. N., 2011, *Intermolecular and Surface Forces*, Academic Press, Burlington, MA.
[3] De Gennes, P.-G., Brochard-Wyart, F., and Quéré, D., 2003, *Capillarity and Wetting Phenomena: Drops, Bubbles, Pearls, Waves*, Springer Science & Business Media, Berlin.
[4] Dirks, J.-H., and Federle, W., 2011, "Fluid-Based Adhesion in Insects–Principles and Challenges," Soft Matter, **7**(23), pp. 11047–11053.
[5] Butler, M. D., and Vella, D., 2022, "Liquid Bridge Splitting Enhances Normal Capillary Adhesion and Resistance to Shear on Rough Surfaces," J. Colloid Interface Sci., **607**, pp. 514–529.
[6] Kohonen, M. M., Geromichalos, D., Scheel, M., Schier, C., and Herminghaus, S., 2004, "On Capillary Bridges in Wet Granular Materials," Phys. A (Amsterdam, Neth.), **339**(1–2), pp. 7–15.
[7] Mitarai, N., and Nori, F., 2006, "Wet Granular Materials," Adv. Phys., **55**(1–2), pp. 1–45.
[8] Kim, H.-Y., and Mahadevan, L., 2006, "Capillary Rise Between Elastic Sheets," J. Fluid Mech., **548**, pp. 141–150.
[9] Bico, J., Roman, B., Moulin, L., and Boudaoud, A., 2004, "Elastocapillary Coalescence in Wet Hair," Nature, **432**(7018), pp. 690–690.
[10] Roman, B., and Bico, J., 2010, "Elasto-Capillarity: Deforming An Elastic Structure With a Liquid Droplet," J. Phys.: Condens. Matter, **22**(49), p. 493101.
[11] Bico, J., Reyssat, É., and Roman, B., 2018, "Elastocapillarity: When Surface Tension Deforms Elastic Solids," Annu. Rev. Fluid Mech., **50**(1), pp. 629–659.
[12] Li, H., Yu, C., and Dai, Z., 2024, "Regimes in the Axisymmetric Stiction of Thin Elastic Plates," Int. J. Mech. Sci., **284**, p. 109740.
[13] Marmur, A., 1993, "Tip-Surface Capillary Interactions," Langmuir, **9**(7), pp. 1922–1926.
[14] Chen, S., and Soh, A., 2008, "The Capillary Force in Micro-and Nano-Indentation With Different Indenter Shapes," Int. J. Solids Struct., **45**(10), pp. 3122–3137.
[15] Dai, Z., Lu, N., Liechti, K. M., and Huang, R., 2020, "Mechanics at the Interfaces of 2D Materials: Challenges and Opportunities," Curr. Opin. Solid State Mater. Sci., **24**(4), p. 100837.
[16] Zheng, W. and Dai, Z., 2025, "Universal Pull-Off Force for Separating a Rigid Sphere From a Membrane," J. Mech. Phys. Solids, **201**, p. 106163.
[17] Zhang, Y., Yin, M., Baek, Y., Lee, K., Zangari, G., Cai, L., and Xu, B., 2020, "Capillary Transfer of Soft Films," Proc. Natl. Acad Sci. U. S. A., **117**(10), pp. 5210–5216.
[18] Shi, C., Jiang, J., Li, C., Chen, C., Jian, W., and Song, J., 2024, "Precision-Induced Localized Molten Liquid Metal Stamps for Damage-Free Transfer Printing of Ultrathin Membranes and 3D Objects," Nat. Commun., **15**(1), p. 8839.
[19] Dong, W., Dai, Z., Liu, L., and Zhang, Z., 2024, "Toward Clean 2D Materials and Devices: Recent Progress in Transfer and Cleaning Methods," Adv. Mater., **36**(22), p. 2303014.
[20] De Volder, M., and Hart, A. J., 2013, "Engineering Hierarchical Nanostructures by Elastocapillary Self-Assembly," Angew. Chem., Int. Ed., **52**(9), pp. 2412–2425.
[21] Li, H., Guo, X., Nuzzo, R. G., and Hsia, K. J., 2010, "Capillary Induced Self-Assembly of Thin Foils Into 3D Structures," J. Mech. Phys. Solids, **58**(12), pp. 2033–2042.
[22] Singh, K., Lister, J. R., and Vella, D., 2014, "A Fluid-Mechanical Model of Elastocapillary Coalescence," J. Fluid Mech., **745**, pp. 621–646.
[23] Kong, A., and Bacca, M., 2022, "A Self-Adhesion Criterion for Slanted Micropillars," Extreme Mech. Lett., **52**, p. 101663.
[24] Li, C., and Tawfick, S., 2025, "Self-Assembly of Lamellae by Elastocapillarity in the Presence of Gravity: Experiments and Modeling," ASME J. Appl. Mech., **92**(2), p. 021004.
[25] Barber, J. R., 2018, *Contact Mechanics*, Vol. 20, Springer, Berlin.
[26] Ciavarella, M., Joe, J., Papangelo, A., and Barber, J., 2019, "The Role of Adhesion in Contact Mechanics," J. R. Soc. Interface, **16**(151), p. 20180738.
[27] Yu, C., Zeng, W., Wang, B., Cui, X., Gao, Z., Yin, J., Liu, L., Wei, X., Wei, Y., and Dai, Z., 2024, "Stiffer Is Stickier: Adhesion in Elastic Nanofilms," Nano Lett., **25**(5), pp. 1876–1882.
[28] Derjaguin, B., 1934, "Untersuchungen Ueber Die Reibung Und Adhaesion, IV: Theorie Des Anhaftens Kleiner Teilchen," Kolloid-Z., **69**, pp. 155–164.
[29] McFarlane, J. S., and Tabor, D., 1950, "Adhesion of Solids and the Effect of Surface Films," Proc. R. Soc. Lond. Ser. A, **202**(1069), pp. 224–243.
[30] Bradley, R. S., 1932, "LXXIX. The Cohesive Force Between Solid Surfaces and the Surface Energy of Solids," Lond. Edinb. Philos. Mag. J. Sci., **13**(86), pp. 853–862.
[31] Maugis, D., 1992, "Adhesion of Spheres: The JKR-DMT Transition Using a Dugdale Model," J. Colloid Interface Sci., **150**(1), pp. 243–269.
[32] Qian, J., Lin, J., and Shi, M., 2016, "Combined Dry and Wet Adhesion Between a Particle and an Elastic Substrate," J. Colloid Interface Sci., **483**, pp. 321–333.
[33] Matthewson, M., 1988, "Adhesion of Spheres by Thin Liquid Films," Philos. Mag. A, **57**(2), pp. 207–216.
[34] Maugis, D., and Gauthier-Manuel, B., 1994, "JKR-DMT Transition in the Presence of a Liquid Meniscus," J. Adhes. Sci. Technol., **8**(11), pp. 1311–1322.
[35] Fogden, A., and White, L. R., 1990, "Contact Elasticity in the Presence of Capillary Condensation: I. The Nonadhesive Hertz Problem," J. Colloid Interface Sci., **138**(2), pp. 414–430.
[36] Goryacheva, I., and Makhovskaya, Y. Y., 2001, "Adhesive Interaction of Elastic Bodies," J. Appl. Math. Mech., **65**(2), pp. 273–282.
[37] Maugis, D., 2000, *Contact, Adhesion and Rupture of Elastic Solids*, Vol. 130, Springer Science & Business Media, Berlin.
[38] Py, C., Reverdy, P., Doppler, L., Bico, J., Roman, B., and Baroud, C. N., 2007, "Capillary Origami: Spontaneous Wrapping of a Droplet With an Elastic Sheet," Phys. Rev. Lett., **98**(15), p. 156103.
[39] Majidi, C., and Adams, G. G., 2009, "A Simplified Formulation of Adhesion Problems With Elastic Plates," Proc. R. Soc. A, **465**(2107), pp. 2217–2230.
[40] Majidi, C., 2009, "Shear Adhesion Between an Elastica and a Rigid Flat Surface," Mech. Res. Commun., **36**(3), pp. 369–372.
[41] Chopin, J., Vella, D., and Boudaoud, A., 2008, "The Liquid Blister Test," Proc. R. Soc. A, **464**(2099), pp. 2887–2906.
[42] Shenoy, V. B., and Gracias, D. H., 2012, "Self-Folding Thin-Film Materials: From Nanopolyhedra to Graphene Origami," MRS Bull., **37**(9), pp. 847–854.
[43] Meng, X., Li, M., Kang, Z., Zhang, X., and Xiao, J., 2013, "Mechanics of Self-Folding of Single-Layer Graphene," J. Phys. D: Appl. Phys., **46**(5), p. 055308.
[44] Wilting, T. J., Essink, M. H., Gelderblom, H., and Snoeijer, J. H., 2021, "How to Unloop a Self-Adherent Sheet," Europhys. Lett., **134**(5), p. 56001.
[45] Sanchez, D. A., Dai, Z., Wang, P., Cantu-Chavez, A., Brennan, C. J., Huang, R., and Lu, N., 2018, "Mechanics of Spontaneously Formed Nanoblisters Trapped by

Transferred 2D Crystals," Proc. Natl. Acad. Sci. U. S. A., **115**(31), pp. 7884–7889.
[46] Ma, J., Kim, J. M., Hoque, M. J., Thompson, K. J., Nam, S., Cahill, D. G., and Miljkovic, N., 2021, "Role of Thin Film Adhesion on Capillary Peeling," Nano Lett., **21**(23), pp. 9983–9989.
[47] Ghorbanfekr-Kalashami, H., Vasu, K., Nair, R. R., Peeters, F. M., and Neek-Amal, M., 2017, "Dependence of the Shape of Graphene Nanobubbles on Trapped Substance," Nat. Commun., **8**(1), p. 15844.
[48] Dai, Z., Sanchez, D. A., Brennan, C. J., and Lu, N., 2020, "Radial Buckle Delamination Around 2D Material Tents," J. Mech. Phys. Solids, **137**, p. 103843.
[49] Rao, Y., Qiao, S., Dai, Z., and Lu, N., 2021, "Elastic Wetting: Substrate-Supported Droplets Confined by Soft Elastic Membranes," J. Mech. Phys. Solids, **151**, p. 104399.
[50] Ronceray, N., Spina, M., Chou, V. H. Y., Lim, C. T., Geim, A. K., and Garaj, S., 2024, "Elastocapillarity-Driven 2D Nano-Switches Enable Zeptoliter-Scale Liquid Encapsulation," Nat. Commun., **15**(1), p. 185.
[51] Mora, S., Phou, T., Fromental, J.-M., Audoly, B., and Pomeau, Y., 2012, "Shape of an Elastic Loop Strongly Bent by Surface Tension: Experiments and Comparison With Theory," Phys. Rev. E, **86**(2), p. 026119.
[52] Glassmaker, N., and Hui, C., 2004, "Elastica Solution for a Nanotube Formed by Self-Adhesion of a Folded Thin Film," J. Appl. Phys., **96**(6), pp. 3429–3434.
[53] Johnson, K. L., Kendall, K., and Roberts, A., 1971, "Surface Energy and the Contact of Elastic Solids," Proc. R. Soc. Lond. A Math. Phys. Sci., **324**(1558), pp. 301–313.
[54] Vella, D., Bico, J., Boudaoud, A., Roman, B., and Reis, P. M., 2009, "The Macroscopic Delamination of Thin Films From Elastic Substrates," Proc. Natl. Acad Sci. U. S. A., **106**(27), pp. 10901–10906.
[55] Derjaguin, B. V., Muller, V. M., and Toporov, Y. P., 1975, "Effect of Contact Deformations on the Adhesion of Particles," J. Colloid Interface Sci., **53**(2), pp. 314–326.
[56] Goryacheva, I., and Makhovskaya, Y. Y., 1999, "Capillary Adhesion in the Contact Between Elastic Solids," J. Appl. Math. Mech., **63**(1), pp. 117–125.
[57] Fan, H., and Gao, Y., 2001, "Elastic Solution for Liquid-Bridging-Induced Microscale Contact," J. Appl. Phys., **90**(12), pp. 5904–5910.
[58] Chen, Z., and Yu, S., 2003, "Capillary Adhesive Contact Between a Spherical Rigid Punch and a Piezoelectric Half Space," J. Appl. Phys., **94**(10), pp. 6899–6907.
[59] Jin, F., Guo, X., and Gao, H., 2013, "Adhesive Contact on Power-Law Graded Elastic Solids: The JKR–DMT Transition Using a Double-Hertz Model," J. Mech. Phys. Solids, **61**(12), pp. 2473–2492.
[60] Jin, F., Tang, Q., Guo, X., and Gao, H., 2021, "A Generalized Maugis-Dugdale Solution for Adhesion of Power-Law Graded Elastic Materials," J. Mech. Phys. Solids, **154**, p. 104509.
[61] Chen, S.-W., Wang, G.-F., and Ciavarella, M., 2025, "Adhesive Contact of Elastic Spherical Shells: Non-Monotonic Thickness Dependence of Pull-Off Force".
[62] Zhao, C., Wan, K.-T., and Shan, W., 2024, "Progressive Adhesion Mechanics of Elastomeric Shells Against a Rigid Substrate: From Thin to Thick," Extreme Mech. Lett., **68**, p. 102140.
[63] Salez, T., Benzaquen, M., and Raphaël, É., 2013, "From Adhesion to Wetting of a Soft Particle," Soft Matter, **9**(45), pp. 10699–10704.
[64] Butler, M., 2020, "Sticking With Droplets: Mathematical Models of Capillary Adhesion," Ph.D. thesis, University of Oxford, Oxford, UK.
[65] Sneddon, I. N., 1960, "The Elementary Solution of Dual Integral Equations," Glasg. Math. J., **4**(3), pp. 108–110.
[66] Sneddon, P., 1995, *Co-Transmission, Neurotransmitter Release and Its Modulation*, Cambridge University Press, Cambridge, UK, pp. 22–37.
[67] Noble, B., 1963, "The Solution of Bessel Function Dual Integral Equations by a Multiplying-Factor Method," Math. Proc. Camb. Philos. Soc., **59**(2), pp. 351–362.
[68] Waters, J., Lee, S., and Guduru, P., 2009, "Mechanics of Axisymmetric Wavy Surface Adhesion: JKR–DMT Transition Solution," Int. J. Solids Struct., **46**(5), pp. 1033–1042.